Bollettino di Geofisica Teorica ed Applicata Vol. 61, n. 1, pp. 89-102; March 2020
DOI 10.4430/bgta0296

Forward modelling of magnetic anomalies in archaeological geophysics: a new software tool

A. Schettino and A. Ghezzi

School of Science and Technology, Geology Division, University of Camerino, Italy

(Received: 6 May 2019; accepted: 5 August 2019)

ABSTRACT We present a new software tool for the analysis and interpretation of archaeological magnetic anomalies, based on classical algorithms of forward modelling and a technique of error assessment. The proposed methodology allows us determining geometry, physical properties, and location of buried archaeological features, as well as the occurrence of fires or other historical events that may have affected the observed magnetic signal. In our approach, the acquisition of total field data, usually in a regular grid arrangement, their reduction to archaeological magnetic anomalies, and the subsequent computer-assisted structural interpretation are accomplished according to a specific workflow that conserves the physical meaning of the magnetic anomalies and excludes any kind of data processing that may change the nature of the anomaly field. In particular, the reduction of the observed total field data to magnetic anomalies is performed subtracting a polynomial representation of the regional field on the basis of a rigorous criterion that separates archaeological anomalies from geological (crustal) contributions, while procedures like line levelling or some kinds of data filtering are excluded to ensure a strict correspondence between magnetic data and the real distribution of magnetisation in the ground.

Key words: archaeological geophysics, magnetic anomalies, forward modelling.

1. Introduction

It is widely accepted that magnetic methods represent one of the most important non–destructive techniques in Archaeology. However, in most cases their application to the detection of buried human structures is qualitative and based on the visual identification of dipolar sources and linear anomalies associated with a variety of archaeological features on vertical gradient maps (e.g. Ciminale and Gallo, 2008). This approach also includes those techniques that require the application of image processing algorithms or special filters for the data enhancement (e.g. Roest *et al*., 1992; Jeng *et al*., 2003; Bescoby *et al*., 2006; Stampolidis and Tsokas, 2012). Although it can provide quickly and efficiently useful information for archaeologists before excavations, this approach does not allow an independent study of the physical sources and the associated anomalous field, which in turn may give important clues about the historical evolution of a settlement. For example, the presence of diffuse coherent thermo-remnant magnetisation (TRM) in the buried structures may be indicative of an event of burning as a consequence of war or natural events.

The possibility of using magnetic data to obtain a physical characterisation of the buried materials relies on the construction of magnetisation models that separate the induced and remnant components starting from the observed total field intensities. To this purpose, it is important to reduce the magnetic intensity readings to anomalies that are the direct expression of the magnetic signal generated by the buried sources. Consequently, it is necessary to avoid any kind of processing (e.g. line levelling) that enhances visualisation sacrificing the physical meaning of the anomaly field, although some basic pre-processing procedures could be still necessary. In general, standard pre-processing consisting into despiking, dropout removal, and decorrugation can remove artifacts associated with the acquisition procedure without changing the physical properties of the field.

Our approach has been described in recent articles (Ghezzi *et al*., 2018; Schettino *et al*., 2018) and meetings. In typical environmental conditions and with a minimum equipment, we divide the survey area in several squared regions having maximum size of ~30×50 m^2 and overlapped edges (0.5 m). For each rectangle, the survey starts with the rapid acquisition of a transversal tie line, which will be used later to build a diurnal drift curve $R(t)$. Taking into account that this line is walked in less than 1 minute, we can consider the corresponding magnetic field readings $T(x,y,t)$ as simultaneous values of the magnetic intensity at the initial time $t = t_0$. A subset of points $c_i = (x_i,y_i)$ along the tie line (one for each subsequent survey line) will be travelled again at later times $t_1 < t_2 < \ldots < t_n$ during the survey. These locations are referred to as the "crossover points". The set of all crossover errors $\varepsilon_i = T(c_i,t_i) - T(c_i,t_0)$ can be considered as a sample of the external field variations with respect to the initial time t_0. Such diurnal drift does not depend on the position at the scale of an archaeological survey, but the sample elements have an uncertainty associated with the positioning errors that affect the locations c_i. Consequently, the diurnal variations curve $R(t)$ relative to the initial time $t = t_0$ must be estimated statistically as a regression curve of the crossover errors ε_i with respect to time. If the survey is completed in a reasonable time interval, a time-independent function, $T(x,y)$, can be obtained subtracting the curve $R(t)$ from the observed data $T(x,y,t)$:

$$T(x,y) = T(x,y,t) - R(t) . \tag{1}$$

This data set represents the total field intensity at survey time, associated with magnetic sources of any depth, including core and crustal contributions. It has a bandwidth whose upper limit λ_{max} is given by the size L of the survey area, $\lambda_{max} = L$, and a lower limit that depends from the data sampling density and their subsequent resampling on a regular grid. The latter is the reciprocal of Nyquist frequency f_n, which is the highest spatial frequency associated with the gridded total field data. This quantity, in turn, is easily obtained by the reciprocal of the grid cell size δs: $f_n = 1/(2\delta s)$, thereby the smallest observable wavelength will be given by: $\lambda_{min} = 1/f_n = 2\delta s$. According to Spector and Grant (1970), the radially averaged power spectrum of $T(x,y)$ in the range $[\lambda_{min}, \lambda_{max}]$ or, more precisely, in the corresponding range of wavenumbers $[k_{min}, k_{max}]$ allows one to identify a series of disjoint wavenumber intervals that are representative of sources at different depths. We will see that this property represents a key aspect of our approach.

The removal of the diurnal drift from the raw magnetic data is followed by the elimination of some short-wavelength artifacts (zig-zags) associated with small errors in the positioning of magnetic readings along the survey lines. For this purpose, we apply the following procedure

[see Fedi and Florio (2003) and references therein]: 1) high-pass filtering of the raw total field data using a high-order Butterworth filter (e.g. $n = 8$) and a cutoff frequency depending on the corrugation wavelength; 2) filtering of the residual grid by a n-degree directional cosine in the survey lines direction; 3) subtraction of the resulting grid from the original raw anomalies. After this step, a set of clean total field grids covering the whole survey area is available and can be used to generate a composite map that is representative of all the internal contributions to the Earth's magnetic field. The assembly of magnetic data sets from individual survey rectangles into a single composite grid is not a simple procedure and requires some caution (Ghezzi *et al*., 2018). In fact, even after the elimination of the diurnal drift relative to the initial time of each rectangle, differences in the acquisition time (and date) determine the formation of discontinuities along the borders of adjacent areas up to few tens nT. Our approach is to allow for small (0.5 m) overlaps at survey time along the edges of each pair of adjacent grids. The average misfit $\langle \delta T \rangle$ along each overlapped region is then used to shift the total field intensity $T(x,y)$ of one of the two grids in order to minimise the border discontinuities:

$$T(x,y) \rightarrow T'(x,y) = T(x,y) - \langle \delta T \rangle \tag{2}$$

where $\langle \delta T \rangle$ can be either positive or negative. Of course, the transformation in Eq. 2 does not change the short wavelength field associated with archaeological features. The final mosaic of total field grids can be used to generate a grid of magnetic anomalies of archaeological interest, ΔT, for the survey area. A rigorous procedure of reduction of magnetic field intensity values $T(x,y)$ to anomalies $\Delta T(x,y)$ is described in Schettino *et al*. (2018) and requires determination of the best polynomial representation $F(x,y)$ of the core and crustal contributions to the observed field, so that:

$$\Delta T(x,y) = T(x,y) - \sum_{n+m \le N} a_n b_m x^n y^m \tag{3}$$

where the reference field $F(x,y) = \sum_{n+m \le N} a_n b_m x^n y^m$ is estimated by least squares polynomial regression over the observed total field values $T(x,y)$. We shall refer to quantities obtained by Eq. 3 to as the "observed anomalies", while the anomalous field vector generated by the buried magnetic sources will be indicated by ΔF. In archaeological geophysics, the reference field $F(x,y)$ should include both the core and crustal (or geological) contributions and exclude any shallow source having archaeological interest. It is possible to prove that an appropriate choice of the polynomial degree N is critical for a correct separation of these sources: low values of N will leave crustal contributions in the observed anomalies, while high values of N will remove part of the bandwidth associated with archaeological sources. In fact, for any selected value of this parameter, Eq. 3 is equivalent to the application of an HP filter to the total field $T(x,y)$, with cutoff wavelength $\lambda(N)$. For some values of the exponent, it could result $\lambda(N) > \lambda_{max}$, which indicates that the reduction to magnetic anomalies by Eq. 3 is ineffective in removing crustal contributions from the observed data. Conversely, for any integer N such that $\lambda(N) < \lambda_{max}$, we have that Eq. 3 will eliminate a segment of the low wavenumbers range from the observed signal. The example in Fig. 1 shows that a reduction to magnetic anomalies by polynomials of degree $N = 3$, 4, or 5 is equivalent to the application of HP filters with cutoff wavelengths $\lambda = 50$, 45, and 30 m,

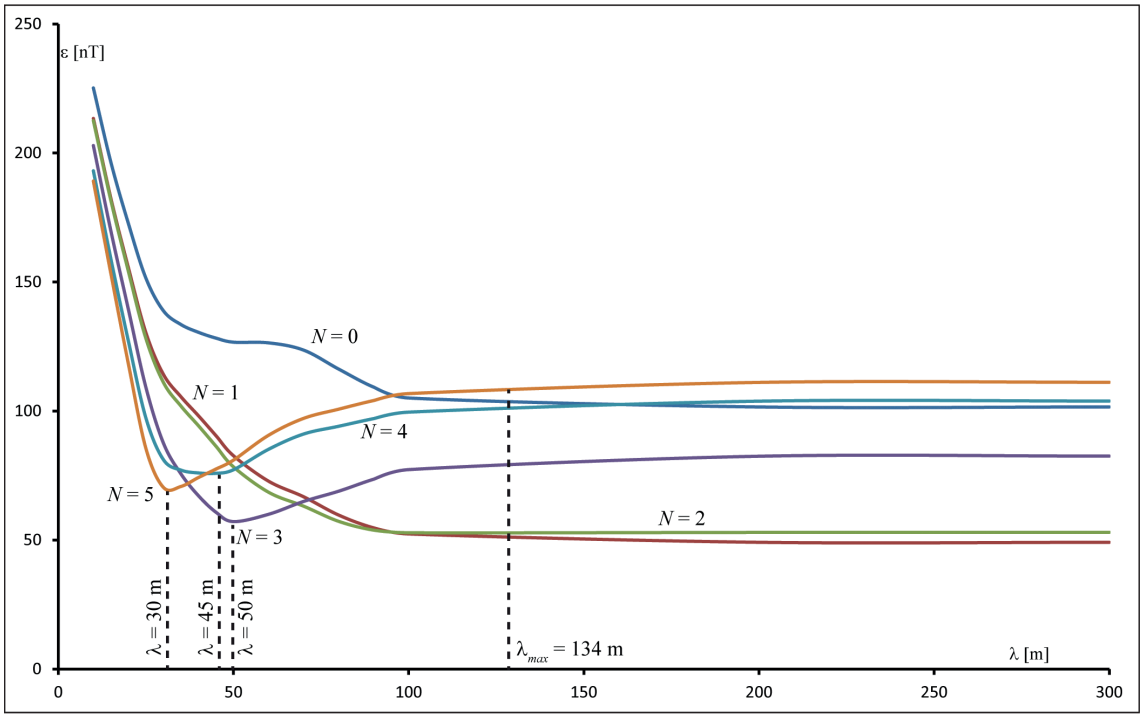

Fig. 1 - Rms error curves $\varepsilon(\lambda,N)$ of the difference between observed anomalies obtained by Eq. 3 using different polynomial degrees N and residual anomalies calculated applying HP filters with cutoff λ to the field $T(x,y)$. The equivalent HP filters corresponding to the application of Eq. 1 are those corresponding to minima of $\varepsilon(\lambda,N)$. Data from Hadrian's Villa, near Rome (Ghezzi *et al*., 2019).

respectively, while for $N = 0$, 1, and 2 the equivalent filter has cutoff wavelength $\lambda(N) > \lambda_{max}$. Consequently, the minimum acceptable value is $N = 3$. This is also the correct initial choice for N, because it reduces to a minimum the risk of removing archaeological information.

The calculation of magnetic anomalies by Eq. 1 is the only way to ensure that the quantities ΔT conserve the physical meaning of being approximately equal to the component of the anomalous field ΔF in the direction of the ambient field vector (Blakely, 1995), which is an essential assumption in the forward modelling of these quantities. Therefore, we can only choose the parameter N through which the reduction in Eq. 3 is performed, not the fact that it must be accomplished in any case. The selection of the reference polynomial surface that is equivalent to the HP filter having the highest cutoff wavelength in the range $[\lambda_{min}, \lambda_{max}]$ will prevent the removal of wavelengths in the archaeological range, although it will not necessarily eliminate all the crustal components. Consequently, it will be anyway suitable to check the resulting anomaly field by a spectral analysis.

To test whether ΔT is effectively the expression of archaeological features and does not include deeper components of geological origin, we can generate the radially averaged power spectrum (Spector and Grant, 1970) of this grid and check that the ensemble with the highest slope has a depth compatible with the maximum depth of the archaeological features (Ghezzi *et al*., 2018; Schettino *et al*., 2018). This kind of analysis also provides a quantitative estimate of the average depths associated with the various sources, which will be used in the subsequent

procedure of forward modelling. Finally, Schettino *et al*. (2018) have shown that it is possible to build an uncertainty grid associated with the field *T* and assign a lower limit to the interpretable anomalies.

The magnetic anomaly grid $\Delta T(x,y)$ can be used in conjunction with a digital elevation model (DEM) of the survey area and a total field uncertainty grid to create a magnetisation model of the underground features that generate the anomalies. To this purpose, we use an interactive trial-and-error procedure that compares at each step the theoretical anomalies associated with the current magnetisation model with the observed anomalies and changes the distribution of magnetisation accordingly. In this paper, we describe such a computer-assisted procedure of analysis and modelling of archaeological magnetic anomalies. We will illustrate the operation of a specialised software tool, ArchaeoMag, which is based on classical forward modelling algorithms and allows for the first time reconstructing interactively the geometry and magnetisation pattern of a buried settlement through a trial-and-error procedure. The program can be freely downloaded at http://www.serg.unicam.it/Downloads.htm. In the next sections, we first describe the operation of ArchaeoMag and the basic steps in forward modelling of archaeological anomalies. Then, we will discuss the potentiality of this approach with some applicative examples.

2. ArchaeoMag: a new software tool in archaeological geophysics

The computer program ArchaeoMag is an MS Windows (v. 7, 8, 10) application designed to operate on UTM georeferenced grids of archaeological anomalies, although it can be also used in local (survey) coordinates. The program assumes that the anomalies have been determined through the correct application of Eq. 3 or a similar method of total field data reduction. In other words, it assumes that the magnetic anomaly amplitudes reflect the true magnetisation of the buried archaeological features. In typical applications, the user specifies an input grid of magnetic anomalies, a DEM grid that encloses the survey area, an uncertainty grid, a colour scale for the representation of the magnetic anomalies, and some ambient parameters. The latter include sensor height, the geomagnetic field parameters (F, D_0, I_0) at survey time, and the soil volume susceptibility χ_0 in SI units. The reference field declination, D_0, and inclination, I_0, are used to calculate model anomalies starting from anomalous field vectors, while the field intensity, F, is used with the soil susceptibility and the susceptibility of the buried objects to determine the induced component of magnetisation M_I. This approach clearly requires a preliminary soil sampling and analysis through a magnetic susceptibility meter. Finally, the survey area parameters (corner coordinates and map resolution) are calculated automatically by the program after the specification of an input magnetic anomaly grid. The basic equations for the calculation of the theoretical anomaly, $\Delta T'$, associated with an object with TRM vector $\boldsymbol{M}_R$ and magnetic susceptibility χ in an ambient field $\boldsymbol{F} = (X, Y, Z)$ read:

$$\begin{cases} X = F \cos I_0 \cos D_0 \\ Y = F \cos I_0 \sin D_0 \\ Z = F \sin I_0 \end{cases} \tag{4}$$

$$\boldsymbol{M}_I = \frac{\chi - \chi_0}{\mu_0}\boldsymbol{F} \equiv \frac{\Delta\chi}{\mu_0}\boldsymbol{F} \tag{5}$$

$$\boldsymbol{M} = \boldsymbol{M}_I + \boldsymbol{M}_R \tag{6}$$

$$\Delta T'(\boldsymbol{r}) = \Delta\boldsymbol{F}(\boldsymbol{r}, \boldsymbol{M}) \cdot \hat{\boldsymbol{F}} \tag{7}$$

where μ_0 is the magnetic permeability in the vacuum, $\mu_0 = 4\pi\times10^{-7}$ H/m, and $\Delta\boldsymbol{F}(\boldsymbol{r},\boldsymbol{M})$ is the anomalous field vector produced at position $\boldsymbol{r}$ by an object with total magnetisation $\boldsymbol{M}$. ArchaeoMag allows one defining five basic classes of shapes and a composite structure, corresponding to common archaeological features: 1) spheres (magnetic dipoles), 2) rectangular prisms, 3) generic vertical prisms, 4) stairways, and 5) cylinders. For any object, the program allows one specifying the minimum and maximum burial depths, the magnetic susceptibility, χ, a cutoff distance beyond which the program does not calculate anomalies (for computing time optimisation), and a remnant magnetisation vector (M_R, D_R, I_R). The calculation of the anomalous field $\Delta\boldsymbol{F}(\boldsymbol{r},\boldsymbol{M})$ is based on optimised versions of classical forward modelling algorithms (Blakely, 1995).

The ArchaeoMag user interface is illustrated in Fig. 2. The program allows us managing several kinds of windows, which can show observed or calculated anomalies, misfit grids, total field uncertainty, or vertical profiles. An open project is associated with a unique observed anomalies window. A project window always displays observed anomalies, while a forward modelling window shows the anomalies calculated from the current magnetisation model. In addition to windows that display scalar fields (i.e. grids), it is possible to open one or more windows that show magnetic or topographic profiles (Fig. 2). The definition of new magnetised blocks, their deletion, or changes to the current parameters is done exclusively in the main project window.

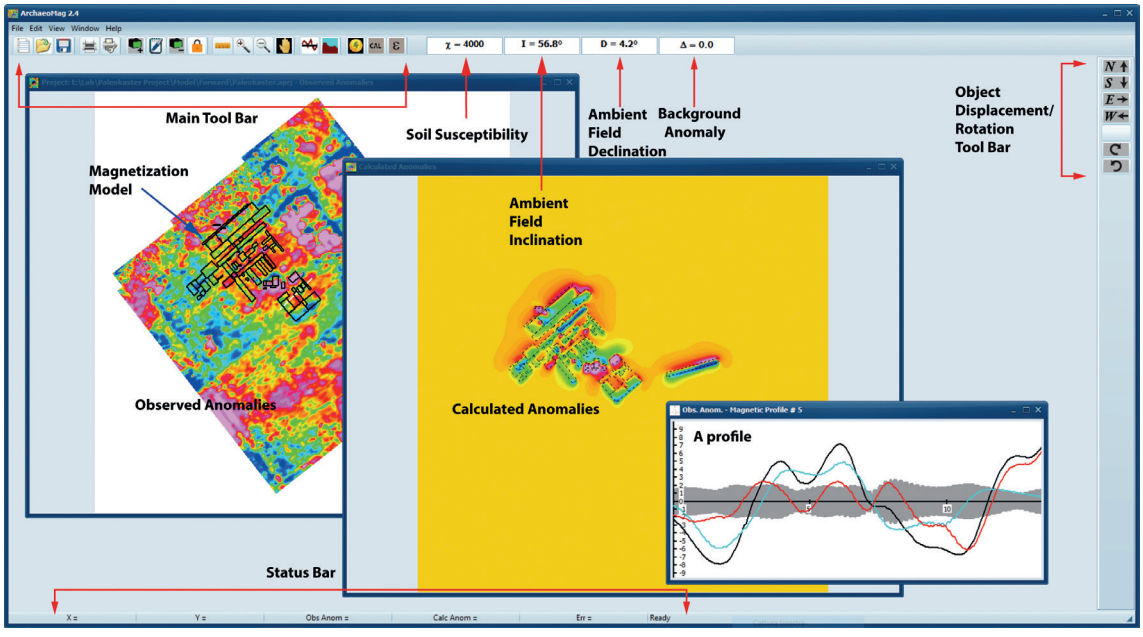

Fig. 2 - ArchaeoMag GUI (graphical user interface) and main windows.

3. Forward modelling procedures

In the forward modelling approach, a magnetisation model of the anomalous field sources is built step by step through a technique that requires repeated comparisons of the theoretical anomalies associated with the current magnetisation model with the anomalies obtained by the observed magnetic intensity values. This is a trial-and-error procedure that involves a sequence of changes to the distribution of magnetisation to reduce progressively the current misfit between model and observed anomalies below the uncertainty level. The main difficulty in this work is represented by the fact that most anomalies have a complex shape that results from the superposition of two or more basic anomalies generated by neighbour bodies. Therefore, it is often necessary to work with several objects at the same time and change simultaneously their parameters at each step during the forward modelling, rather than proceed with one block at a time. In general, the first step in the definition of a new magnetised block is a guess about its geometry on the basis of the anomaly shape, while the burial depth is assigned by quantitative methods such as Euler deconvolution (Reid *et al*., 1990; Desvignes *et al*., 1999) and radially averaged power spectrum analysis (Spector and Grant, 1970). As mentioned in the previous section, in ArchaeoMag the physical parameters of the sources are specified assigning intensity and direction of the TRM vectors and a magnetic susceptibility. TRM represents the principal component of the total magnetisation vector in most of the situations that can be studied by magnetic methods. For example, limestone walls with negligible magnetic susceptibility and embedded in a normal soil with susceptibility around 300×10^{-6} SI acquire an induced magnetisation $M_I = \Delta\chi F/\mu_0 = 0.01$ A/m, which will produce an anomaly with maximum amplitude of less than 3 nT when the burial depth is 0.5 m. In these conditions, only fired structures, pottery, kilns, etc. can be detected by magnetic methods. However, in the unusual case of a very magnetic soil with susceptibility $\chi_0 = 3000$ nT, the same walls would produce an anomaly with a negative peak below -25 nT. In general, the observation of anomalies generated by induced magnetisation requires one or more among the following conditions: 1) a strong susceptibility contrast with the surrounding soil; 2) a random arrangement of TRM components (e.g. a random orientation of magnetite grain spins in a paramagnetic matrix, a random build-up of bricks, etc.); 3) a low Koenigsberger ratio $Q = M_R/M_I$; 4) the absence of nearby objects with a significant TRM component. The most common archaeological feature with strong induced magnetisation and associated high-amplitude anomalies is represented by historical iron artifacts (Bevan, 2002). In normal soil conditions, remnant magnetisation produces high-amplitude anomalies when the materials have high Koenigsberger ratio or, more often, when the archaeological structures are fired materials (e.g. bricks) or materials that have been fired at a later time during historical or natural events. When the modelling of an anomaly requires a TRM component, the declination and inclination of the TRM are chosen on the basis of the strike of the symmetry axis of the anomaly (Fig. 3) and taking into account of the relative amplitudes of the positive and negative peaks (Fig. 4).

It is good practice to start the modelling of a magnetic source by generating several profiles through the corresponding anomaly and having different strikes. Then, the investigator will choose initial shape and magnetisation parameters of one or more objects that are assumed to represent adequately the source. At each subsequent step, the profiles show the observed and calculated anomalies along the profile traces, an error curve (observed minus theoretical anomaly values), and an uncertainty band (Fig. 5) that in principle should envelop the error curves at

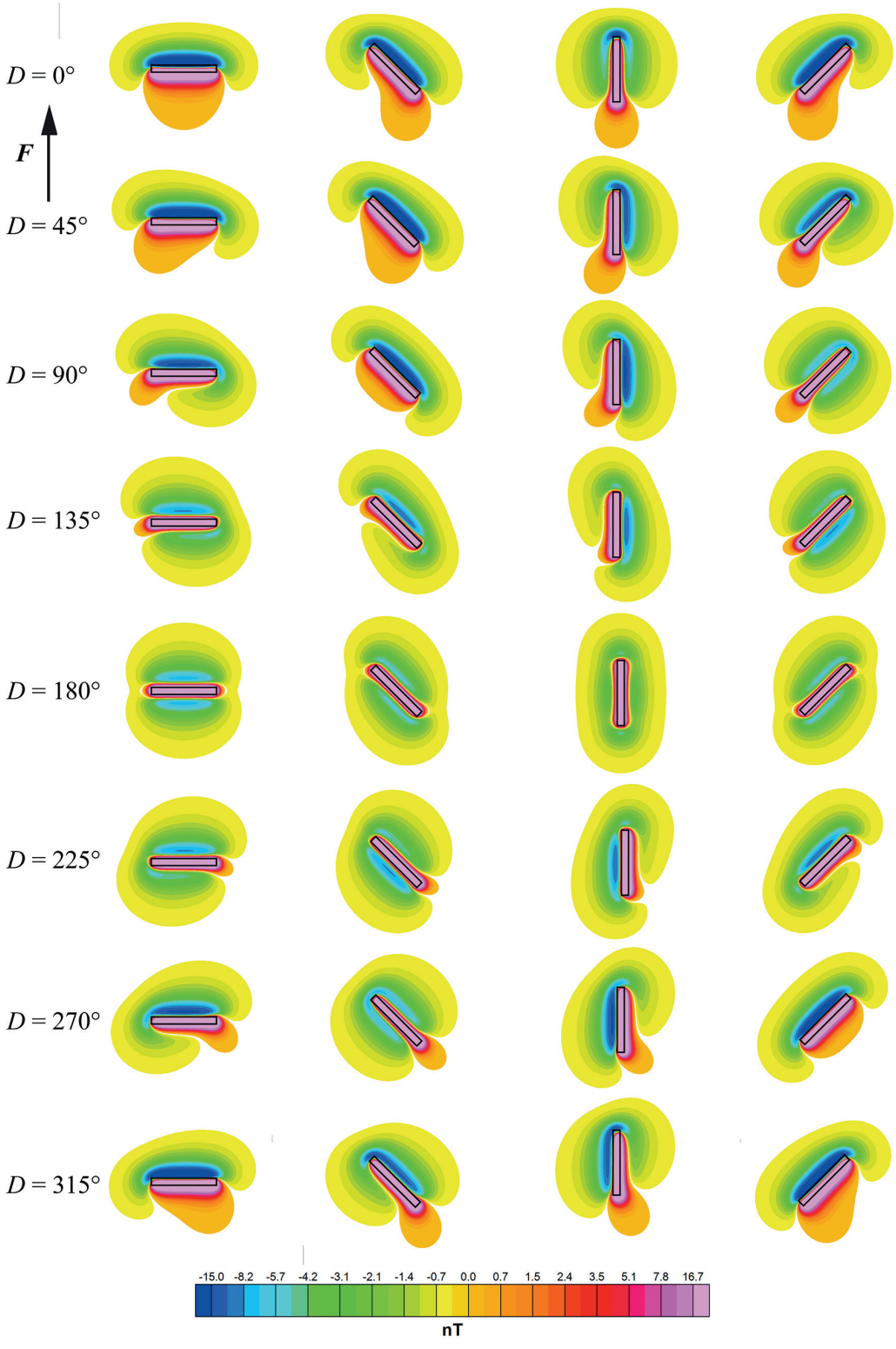

Fig. 3 - Effect of declination. A wall (black rectangle) has TRM inclination $I = 55°$ and $M_R = 1$ A/m. It is assumed that the ambient field has intensity $F = 46{,}483$ nT, declination $D_0 = 0°$, inclination $I_0 = 55°$ and that the sensor height is 0.3 m above a flat terrain. In this example, the susceptibility contrast is zero.

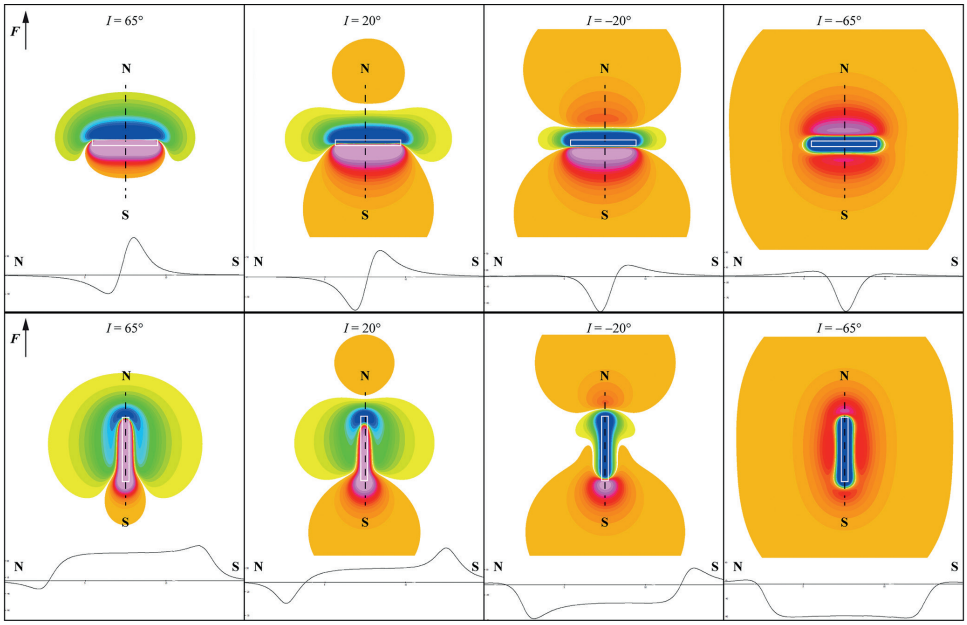

Fig. 4 - Effect of inclination. A wall (white rectangle) has TRM declination $D = 0°$ and $M_R = 1$ A/m. It is assumed that the ambient field has intensity $F = 46{,}483$ nT, declination $D_0 = 0°$, inclination $I_0 = 55°$ and that the sensor height is 0.3 m above a flat terrain. In this example, the susceptibility contrast is zero. The profiles show model anomalies along the N-S traces indicated in the upper panel (dashed lines).

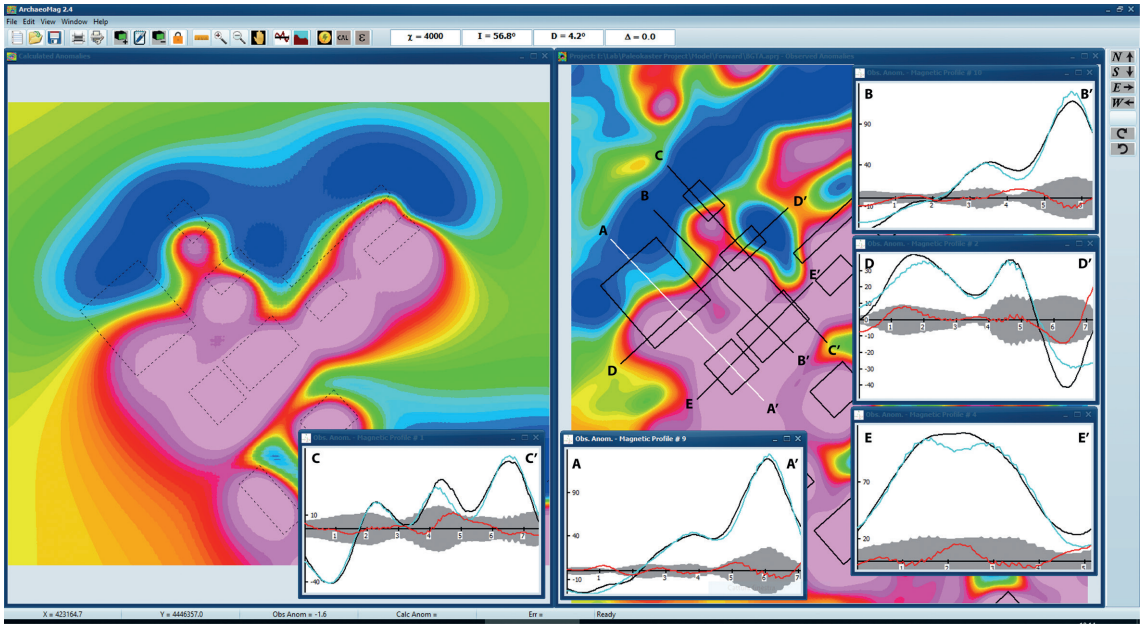

Fig. 5 - A stage in the forward modelling of a complex anomaly, resulting from the superposition of several basic anomalies generated by rectangular prisms. The left window shows calculated anomalies, while the observed data are displayed in the background window to the right. The magnetised blocks are shown as empty rectangles with a black boundary. Five profiles have been traced to check the quality of the fit along several directions. The blue and black curves show calculated and observed anomalies, respectively, while the red line shows the error curve. The grey band is the local uncertainty. Profile A–A´ shows a very good fit, with only a small portion out of the uncertainty, while profiles B–B´, D–D´, and E–E´ still require some work.

the end of the procedure. As mentioned above, an investigator reduces the error curve within the uncertainty limits by an interactive trial-and-error procedure that modifies repeatedly the magnetisation model. At each iteration, the magnetisation parameters and eventually shape and size of the objects, that compose the source, are adjusted to progressively minimise the mismatch between the model and observed anomalies along the profiles. It is important to note that the final magnetisation model is not necessarily what we could find by direct excavation, because of the intrinsic ambiguity of potential field data. However, the available archaeological information can provide important constrains, thereby allowing a realistic reconstruction of the buried settlement. In the example of Fig. 5 (a small portion of a 3rd century Roman fortress in southern Albania), the existence of several blocks with significant TRM, which contribute to the formation of a complex anomaly, is suggested by the sequence of relative maxima and minima with amplitudes of several tens nT along any profile.

Most of these blocks has been modelled with a TRM declination of 330°, while the remaining declination values are in the relatively narrow range between 330° and 10°. The TRM inclinations seem to fall either between 25° and 35° or between 65° and 75°. All these archaeomagnetic directions are not compatible with the paleosecular variations (PSV) curve of Tema and Kondopoulou (2011) for the Balkan area. Consequently, the magnetised materials are not in place and it is reasonable to assume that the magnetisation is generated by an assemblage of bricks (Bevan, 1994). In the following section, we will illustrate with few significant examples the potentiality of the forward modelling approach in the solution of complex situations.

4. Applicative examples

A first interesting example of the ArchaeoMag modelling potentialities comes from a sector of Hadrian's Villa, a UNESCO World's heritage site near Rome (Ghezzi *et al*., 2019). This archaeological site lies on a substratum composed of an ignimbrite tuff massive deposit with very high magnetic susceptibility $\chi = 18{,}127$ [$\times 10^{-6}$] and strong TRM: $M_R = 4.82$ A m^{-1}, $D = 4.1°$, $I = 72.8°$.

A complex system of tunnels was dug in the tuff to link different zones of this Roman villa. Some of these tunnels are known and can be walked, but most them still wait to be mapped. Fig. 6 shows the strong anomalies that can be observed in the Plutonium-Inferi area, associated exclusively with the presence of tunnels, skylights, and ditches carved in the tuff. In this area, the tuff is also covered by a ~0.3 m layer of very magnetic soil with susceptibility $\chi_0 = 9500$ [$\times 10^{-6}$].

The magnetisation model shown in Fig. 6 does not include archaeological features buried in the topsoil layer, thereby the fit between calculated and observed anomalies is quite coarse. However, it explains most of the high-amplitudes anomalies observed in this area. To set up the model, preliminary paleomagnetic and magnetic susceptibility sampling and analysis were performed on the tuff and soil units below the archaeological site. These two layers were modelled as rectangular prisms encompassing the whole area at depths 0.3-5.0 and 0.0-0.3 m respectively. To model empty tunnels and skylights in the tuff, we used rectangular prisms and cylinders, respectively, embedded in the tuff unit and with opposite magnetisation parameters: $M_R = -4.82$ A m^{-1}, $D = 4.1°$, $I = 72.8°$, $\chi = -18{,}127$ [$\times 10^{-6}$]. Similarly, to create a model of soil-filled ditches carved in the tuff, we defined vertical prisms that overlapped the uppermost part of the tuff layer with opposite TRM and susceptibility $\chi = \chi_0 - 18{,}127$ [$\times 10^{-6}$] = -8627 [$\times 10^{-6}$].

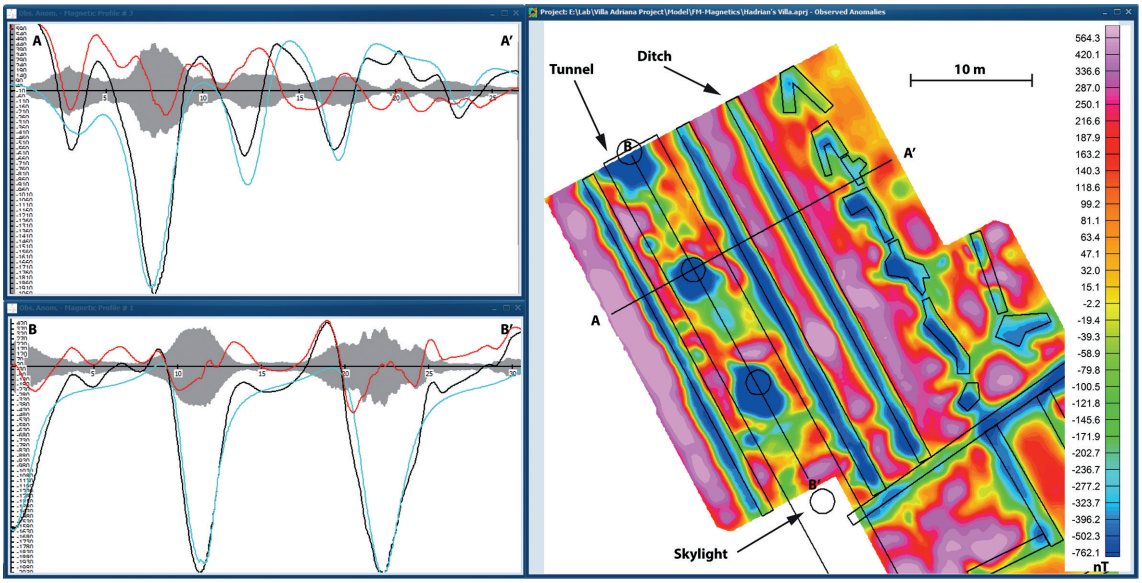

Fig. 6 - Observed magnetic anomalies and magnetisation model (black lines) of the substratum of a portion of the Plutonium-Inferi Complex at Hadrian's Villa (Ghezzi *et al*., 2019), exluding archaeological structures buried in the topsoil.

The next example comes from the already mentioned Roman fortress in southern Albania. Differently from the situation illustrated in Fig. 5, we now focus on the induced magnetisation of the limestone walls of the barracks. This is a good example structures with no TRM and negligible induced magnetisation, which can be detected only thanks to the negative contrast with a soil having strong magnetic susceptibility (Fig. 7).

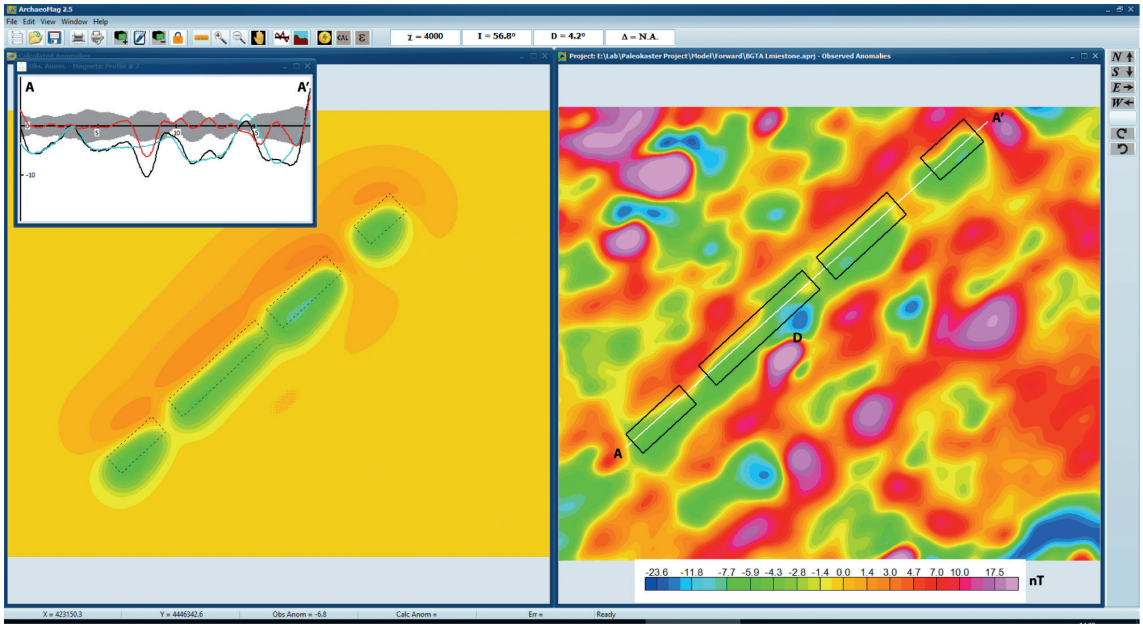

Fig. 7 - Observed (right window) and calculated (left window) magnetic anomalies associated with an interrupted barrack wall (black rectangles). The profile shows a good fit between the two lines, with the exception of a zone where the dipolar source **D** generates a more strongly negative signal.

In this second example, the soil has magnetic susceptibility χ_0 = 4000 [×10^{-6}], while the limestone walls are assumed to have $M_R = 0$ and $\chi = 0$. By Eq. 4, with an ambient field intensity F = 46,483 nT at survey time, this implies an induced magnetisation $M_I \cong -0.15$ A m^{-1}. Assuming burial depths between 50 and 60 cm, as suggested by a spectral analysis of the anomalies, we obtain magnetic anomalies with amplitudes between –10 and +3 nT in agreement with the observation.

The last example, which comes from an archaeological site near Macerata, Italy, illustrates the importance of modelling for the determination of the classes of archaeological materials that contribute to the formation of magnetic anomalies. Fig. 8 shows a large anomaly with peak amplitude of ~600 nT. A good fit of this anomaly can be obtained assuming induced magnetisation and no TRM, with a very large susceptibility χ = 500,000×10^{-6}. This suggests that a large metallic object is buried in this location and the magnetisation model shows that the burial depth is close to ~1 m. Without a quantitative modelling of the anomaly, it would have been impossible to establish the nature of the artifact that has generated this signal.

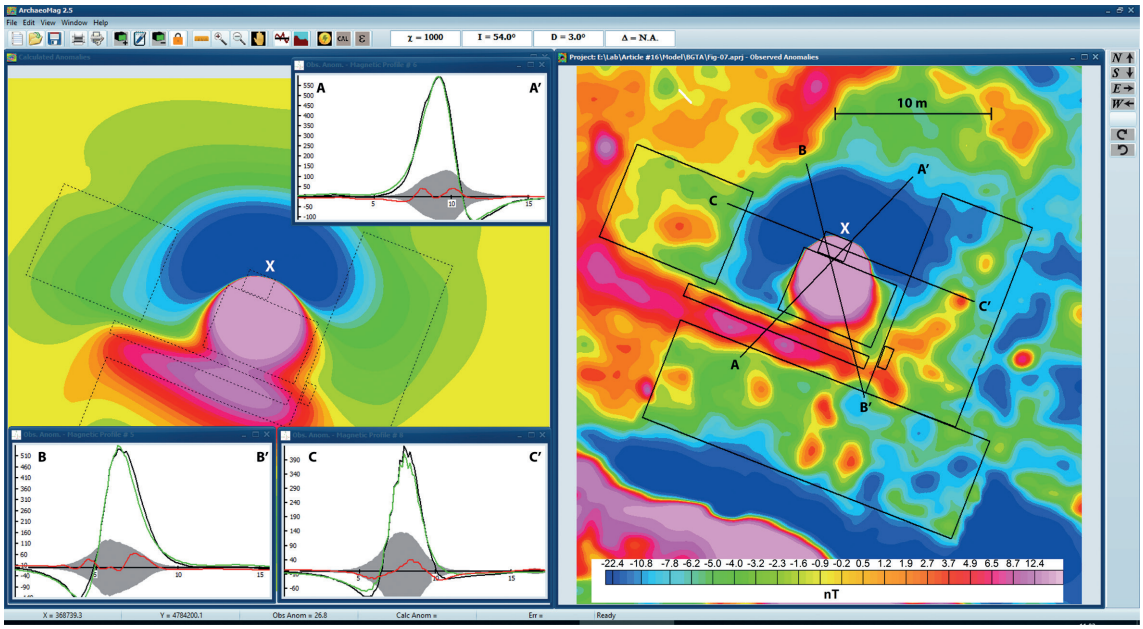

Fig. 8 - Observed (right window) and calculated (left window) magnetic anomaly associated with a large metallic object, having horizontal dimensions 1.8×1.4 m^2 and 0.6 m thickness (small black rectangle X), buried at 0.9 m. The model susceptibility is χ = 500,000×10^{-6}, compatible with an iron alloy.

5. Discussion

The approach presented in the previous sections allows one creating reliable magnetisation models of archaeological sites, allowing for a better representation of the buried structures with respect to the simple visual detection of magnetic lineaments. An important aspect is that a model of the archaeological structures can be built even in the case of complex topography, granted that appropriate acquisition and processing of total field data have been performed and that a digital elevation model of the survey area is available. The possibility to model a TRM component in

addition to the induced magnetisation is an important feature of ArchaeoMag, which could be used, in some circumstances, to estimate the age of firing events and help reconstructions of the historical development of a settlement.

In order to obtain reliable results, ArchaeoMag requires a careful procedure of acquisition of total magnetic field intensities, accompanied by an estimate of the positioning errors and by a technique for the removal of the diurnal drift. In addition, the subsequent data processing should reduce the magnetic field intensities to anomalies that are exclusively representative of archaeological sources. To this purpose, it is recommended to avoid any kind of data enhancement through special filters, because these techniques irremediably change the power spectrum of the magnetic anomalies. In general, the modelling techniques presented here assume that the anomalies have a definite physical meaning and represent at any point the projection of the anomalous field vector onto the reference field direction (Blakely, 1995). In addition, it is assumed that their bandwidth excludes the presence of geological sources. Consequently, with the exception of destriping, the application of filters to the magnetic anomaly grids that are involved in the computer-assisted phase of modelling should be avoided.

6. Conclusion

In the previous sections, we have presented a new approach to the modelling of magnetic data in archaeological geophysics, which is based on a computer-assisted, interactive procedure for the definition and testing of magnetisation distributions associated with buried archaeological features. In this approach, total field data are acquired, filtered, and reduced to archaeological anomalies according to standard procedures. Then, an interactive forward modelling software, ArchaeoMag, is used to create and edit magnetisation models of buried settlements. ArchaeoMag is written in C++ and does not rely on external runtime libraries such as MatLab®. In addition, it allows one distinguishing between induced and NRM components of magnetisation, thereby allowing for a fine calibration of the model and possibly a dating of firing events.

Acknowledgements. This work was initially presented at the 36th GNGTS meeting, Trieste, 14-16 November 2017. We would thank two anonymous reviewers for their useful suggestions.

REFERENCES

Bescoby D.J., Cawley G.C. and Chroston P.N.; 2006: *Enhanced interpretation of magnetic survey data from archaeological sites using artificial neural networks*. Geophys., **71**, H45-H53.

Bevan B.W.; 1994: *The magnetic anomaly of a brick foundation*. Archaeolog. Prospect., **1**, 93-104.

Bevan B.W.; 2002: *The magnetic properties of archaeological materials, 2nd ed*. Geosight, Tech. Report n. 5, 13 pp., doi: 10.13140/RG.2.1.3505.5603.

Blakely R.J.; 1995: *Potential theory in gravity and magnetic applications*. Cambridge University Press, Cambridge, UK, 441 pp.

Ciminale M. and Gallo D.; 2008: *High-resolution magnetic survey in a quasi-urban environment*. Near Surf. Geophys., **6**, 97-103.

Desvignes G., Tabbagh A. and Benech C.; 1999: *The determination of the depth of magnetic anomaly sources*. Archaeolog. Prospect., **6**, 85-105.

Fedi M. and Florio G.; 2003: *Decorrugation and removal of directional trends of magnetic fields by the wavelet transform: application to archaeological areas*. Geophys. Prospect., **51**, 261-272.

Ghezzi A., Schettino A., Tassi L. and Pierantoni P.P.; 2018: *Magnetic modelling and error assessment in archaeological geophysics: the case study of Urbs Salvia, central Italy*. Ann. Geophys., **61**, 1-40, doi: 10.4401/ag-7799.

Ghezzi A., Schettino A., Pierantoni P.P., Conyers L., Tassi L., Vigliotti L., Schettino E., Melfi M., Gorrini M.E. and Boila P.; 2019: *Reconstruction of a segment of the world's heritage Hadrian's Villa tunnels network by integrated GPR, magnetic-paleomagnetic, and electric resistivity prospections*. Remote Sens., **11**, 1739, doi: 10.3390/rs11151739.

Jeng Y., Lee Y.L., Chen C.Y. and Lin M.J.; 2003: *Integrated signal enhancements in magnetic investigation in archaeology*. J. Appl. Geophys., **53**, 31-48.

Reid A.B., Allsop J.M., Granser H., Millett A.T. and Somerton I.W.; 1990: *Magnetic interpretation in three dimensions using Euler deconvolution*. Geophys., **55**, 80-91.

Roest W.R., Verhoef J. and Pilkington M.; 1992: *Magnetic interpretation using the 3-D analytic signal*. Geophys., **57**, 116-125.

Schettino A., Ghezzi A. and Pierantoni P.P.; 2018: *Magnetic field modelling and analysis of uncertainty in archaeological geophysics*. Archaeolog. Prospect., **26**, 137-153, doi: 10.1002/arp.1729.

Spector A. and Grant F.S.; 1970: *Statistical models for interpreting aeromagnetic data*. Geophys., **35**, 293-302.

Stampolidis A. and Tsokas G.N.; 2012: *Use of edge delineating methods in interpreting magnetic archaeological prospection data*. Archaeolog. Prospect., **19**, 123-140.

Tema E. and Kondopoulou D.; 2011: *Secular variation of the Earth's magnetic field in the Balkan region during the last eight millennia based on archaeomagnetic data*. Geophys. J. Int., **186**, 603-614.

Corresponding author: Antonio Schettino
School of Science and Technology, Geology Division, University of Camerino
Via Gentile III da Varano, 62032 Camerino (MC), Italy
Phone: +39 0737 402641; e-mail: antonio.schettino@unicam.it